Analysis of NonMagnetic Spring Plate

KM Galib*, Subrato Roy**, Md Faiaz Arman Talukder Tonmoy***
*(Mechanical Engineering, University of Wyoming, Queens, New York
Email: Lgalib6@gmail.com)
** (Mechanical Engineering, Washington State University, Vancouver, Washington
Email: subrato.roy@wsu.edu)
*** (Mechanical Engineering, University of Alberta, Alberta, Canada
Email: mdfaiaza@ualberta.ca)

Abstract:

A nonlinear spring plate is a complex formed geometry, which acts as a momentary contact switch by snap through behavior. Nonlinear spring plates have a large number of applications in the medical, military, aviation and electronics industries. Spring plates are normally manufactured from 301 stainless steel. Since spring plates made of such materials could alter their behavior in a magnetic environment, nonmagnetic materials have been studied in this work as a potential candidate for nonlinear spring plates operating in magnetic conditions. Upon analyzing the magnetic properties of several materials, it was found that grade 5 titanium alloy and aluminum bronze are potential candidates to replace the magnetic material of nonlinear spring plates. Observing the force-displacement curves it was found that titanium alloy has the lowest trip force compared to other materials. However, fatigue analysis of the spring plates revealed that titanium alloy has the lowest life cycle compared to other materials, which agrees with the testing performed by the manufacturer. Finite element analysis has been performed to investigate the lower life cycle of titanium alloy spring plates

Keywords — **Nonmagnetic, spring plate, fatigue analysis, plastic deformation, micro-cavities, fracture energy**

I. INTRODUCTION

Nonlinear spring plates are critical components used as momentary contact switches that complete a circuit when pressed and revert to an open position upon release. These plates typically fail due to dome cracking after repeated cycles, a result of fatigue from normal use rather than immediate mechanical failure. They are manufactured from rolling sheets via a forming process, with damage accumulation beginning at the onset of plastic deformation. Understanding the forming mechanisms and the factors contributing to fatigue is vital for improving their durability. Various numerical models have been proposed to analyze crack initiation and propagation during the forming process. For instance, Bacha et al. [1] demonstrated that the crack path is controlled by stress and strain fields, with damage based on plastic strain accumulation. Gurson [2], Tvergaard, and Needleman [3] introduced a model for crack propagation via micro-cavity evolution, later refined by Nashon and Hutchinson [4] and Nielson and Tvergaard [5] to include shear effects for better predictions under low-stress triaxiality.

Residual stresses induced during punching also play a significant role in spring plate performance, as analyzed by M. Achouri et al. [6] and Smith et al.

[7]. Changes in force-displacement behavior due to these stresses were observed in actuation models. K.M. Galib et al. [8] used finite element analysis (FEA) to compare stress distributions in composite materials. Fatigue life is influenced by material properties such as ductility, tensile strength, and elasticity. Manson and Hirschberg [9] highlighted the importance of these properties, while Subrato et al. [10, 11] provided fatigue life estimations based on variations in yield properties. The universal slope equation, modified by Manson and Muralidharan [12], was used to calculate minimum fatigue life cycles.

II. Fatigue Analysis and Magnetization Effects in Nonlinear Spring Plates

Fatigue performance depends heavily on stress distribution and material characteristics. Lucas and Konieczny [13] demonstrated the role of grain size in enhancing tensile strength, and Shabnam et al. [14] showed how improved tensile strength boosts the fatigue limit of Ti-6Al-4V. In magnetic environments, the ferromagnetic properties of 301 stainless steel, commonly used in spring plates, can degrade performance. While the magnetization effect is minor, strong magnetic fields necessitate replacing 301 stainless steel with nonmagnetic alternatives like titanium, copper, or beryllium alloys, without compromising mechanical performance. The mechanical and magnetic properties of these materials are compared in this study.

Further, advancements in magnetic applications such as nanocrystalline materials (McHenry and Laughlin [15]), inclined permanent magnets for load-independent resonance (Robertson [16]), and elasto-magnetic suspensions (Bonisoli [17]) were reviewed. Composite permanent magnet designs (Kneller [18]) and the impact of tempering on spring steel fatigue properties (Lee [19], Nam et al. [20]) were also studied. Processes like oil quenching for spring steel (Hton et al. [21]) and silicon nitride ceramics for extreme conditions (Iyash et al. [22]) revealed significant potential for improving fatigue performance. Numerical methods from prior studies, including those by A. Hossain [23], Subrato et al. [24], and Favero et al. [25], confirmed ANSYS as an optimal tool for this analysis due to its precision and flexibility. This comprehensive approach enhances understanding of fatigue behavior and material performance under varying conditions, providing insights for material selection and spring plate design improvements.

III. Method

The simulation model of a nonlinear tactile dome was developed using the ductile damage criterion. This criterion assumes that the progressive degradation of material stiffness ultimately leads to material failure. It is characterized by mesh independency and does not restrict the evolution of damage through the initiation phase. Multiple damage mechanisms act simultaneously and independently on the material, contributing to the overall degradation process.

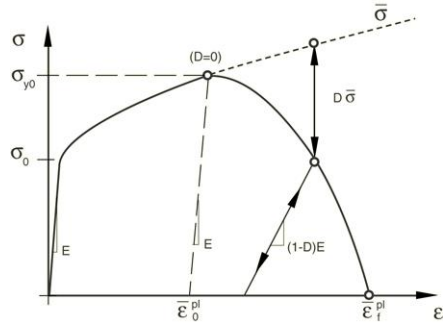

Fig. 1 Stress-strain response under damage criteria [13]

The solid line in Figure 1 represents the damaged stress-strain response, while the dashed line represents the response in the absence of damage.

In the Figure 1,

σ_{y0} = yield stress

ε_0^{pl} = equivalent plastic strain

ε_f^{pl} = equivalent plastic strain at failure

D = overall damage variable

In figure 1, equivalent plastic strain, ε_f^{pl} reaches its value, when the overall damage variable, D is equal

to 1. At the damage initiation, stress-strain relation no longer accurately represents material behavior. When the damage is initiated, results become much dependent on mesh refinement, consequently results start losing accuracy. So Hillerborg [26] proposed a stress-displacement relation instead of a stress-strain relation to reduce mesh dependency, in a response of damage initiation. In this method stress-displacement is characterized to the softening response rather than stress-strain response.

Ductile damage model assumes that at the onset of damage, the equivalent plastic strain is a function of stress traixiality and strain rate,

$$\varepsilon_D^{pl} = f(\eta, \varepsilon^{pl}) \qquad (1)$$

Plastic strain at failure cannot be used as a material parameter [27]. And stress triaxiality is defined as a ratio of hydrostatic stress to von Mises stress,

$$\eta = -\frac{p}{q} \qquad (2)$$

In ductile damage criteria, ω_D is a damage variable, which is computed in every iteration of the analysis. The criterion for damage initiation is met when the following condition is satisfied,

$$\omega_D = \int \frac{d\varepsilon^{pl}}{\varepsilon_D^{pl}(\eta, \varepsilon^{pl})} \qquad (3)$$

The ductile damage model in Abaqus is controlled by specific damage parameters. For the dynamic analysis of the forming model, the Abaqus/Explicit solver was utilized. The forming model consists of four parts, with a quarter-symmetric configuration achieved by applying appropriate constraints to each part. The blank was modeled using the linear reduced integrated element C3D8R, while the rigid elements R3D8 were used for the top punch, bottom punch, and die. In this model, the blank was assumed to be an elastoplastic material, while the rigid parts were treated as elastic materials. The damage parameters used in the model are listed in Table 1.

TABLE I MATERIAL PROPERTIES

Parameters	**301 stainless steel**	**Ti-6Al-4V**	**Aluminum bronze**
Modulus of elasticity (ksi)	29080	16500	15500
Poisson's ratio	0.3	0.35	0.3
Ultimate tensile strength (ksi)	163.312	160	32
Fracture energy (in.lbf)	65	80	40
Stress triaxiality	0.5	0.489	0.6
Fracture strain	0.4	0.44	0.55
Ductility	0.45	0.25	0.4
Modulus of elasticity (ksi)	29080	16500	15500

The assembled parts of the forming model are shown in Figure 2. Given that this model involves multiple body contacts, the contact definitions between the bodies are critical for the analysis. Thus, tangential and normal interaction properties were specified for the body contacts. Tangential interaction was defined as frictionless, and a hard penalty was applied to normal interactions. The punching process was controlled by applying a constant velocity to the top punch in the analysis.

IV. Actuation models

The ductile damage model in Abaqus is controlled by specific damage parameters. For the dynamic analysis of the forming model, the Abaqus/Explicit solver was utilized. The forming model consists of four parts, with a quarter-symmetric configuration achieved by applying appropriate constraints to each part. The blank was modeled using the linear reduced integrated element C3D8R, while the rigid elements

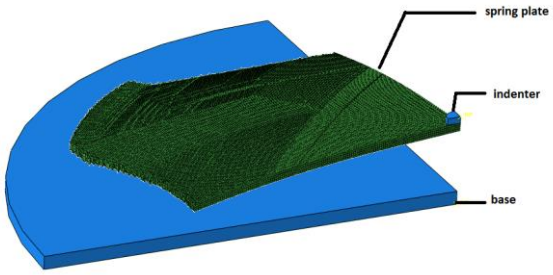

Fig. 3 Assembled parts of forming model

R3D8 were used for the top punch, bottom punch, and die. In this model shown in figure 3, the blank was assumed to be an elastoplastic material, while the rigid parts were treated as elastic materials. The damage parameters used in the model are listed in Table 1. The assembled parts of the forming model are shown in Figure 2.

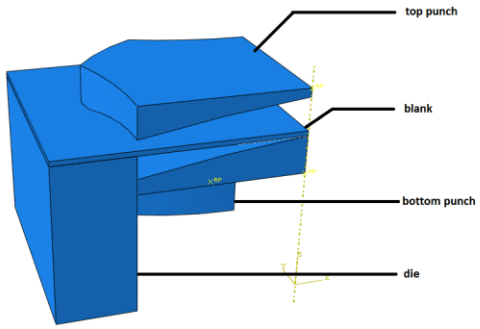

Fig. 2 Assembled parts of forming model

Given that this model involves multiple body contacts, the contact definitions between the bodies are critical for the analysis. Thus, tangential and normal interaction properties were specified for the body contacts. Tangential interaction was defined as frictionless, and a hard penalty was applied to normal interactions. The punching process was controlled by applying a constant velocity to the top punch in the analysis.

V. Fatigue model

The modified universal slope equation, used for fatigue calculation, is expressed as follows::

$$\Delta\varepsilon = 0.0266D^{0.115}\left[\frac{S_u}{E}\right]^{-0.53} N_f^{-0.53} + 1.17 \left[\frac{S_u}{E}\right]^{0.832} N_f^{-0.09} \quad (4)$$

In this equation, equation $\Delta\varepsilon$ is the total strain per cycle, D is the ductility, S_u is the ultimate tensile strength and N_f is the fatigue life. This equation presents challenges due to the iterative solution technique required, which complicates its application. To address this, an alternative method was developed to bypass this complexity. In this approach, the material properties of a spring plate were subjected to fatigue analysis and substituted into the universal slope equation, along with an input vector for fatigue life. As a result, an associated strain vector was generated. Subsequently, the associated strains and fatigue life were fitted to a power law, yielding a simplified power law equation applicable to different materials. Analysis of the failed samples provided by the manufacturer revealed that cracks initiate at the crotch region of the nonlinear spring plates, as shown in Figure 4.

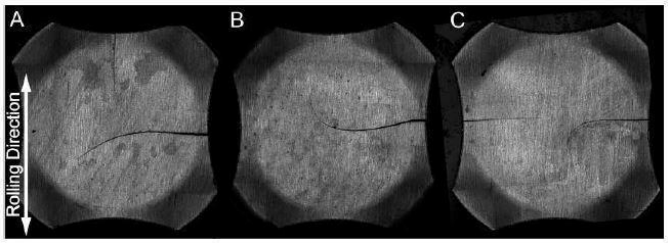

Fig. 4 Failed nonlinear spring plates [15]

The actuation model was used to simulate crack propagation initiation at the nonlinear dome switch in the model with using abacus, python and matlab, shows the crack initiation Figure 5.

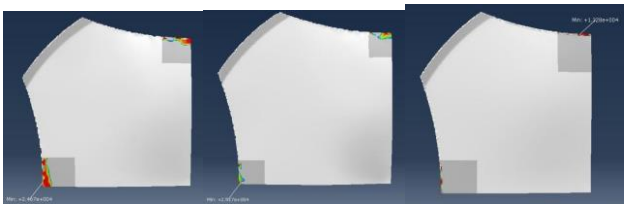

301 stainless steel Aluminum-bronze Ti-6Al-4V

Fig. 5 Fatigue life analysis in crotch region

VI. Nonmagnetic material selection

TSpecial attention was given in this study to the selection of a nonmagnetic material for the spring plates, where magnetic properties are undesirable. The magnetic characteristics of a material are described by the following equations:

$$M = \chi_m H \quad (5)$$

$$B = \mu_0 H + \mu_0 M \quad (6)$$

In this equation B is the magnetic flux density, H is magnetic the field strength, M is the magnetization, μ_0 is the permeability and χ_m is the magnetic susceptibility. The external magnetic field (H) induces magnetic flux density (B). Magnetic moment (M) of a material tends to align with the external magnetic field. How a material would have responded in a magnetic work condition characterized by the internal material parameters permeability, μ_0 and magnetic susceptibility χ_m. Different nonmagnetic materials are compared in terms of these parameters in table 2 alongside 301 stainless steel. Various nonmagnetic materials are compared based on these parameters in Table 2, alongside 301 stainless steel.

TABLE 2 COMPARISON OF MAGNETIC PROPERTIES

Material	Type	Volume susceptibility, χ_m	Permeability, μ_0
301 stainless steel	Ferromagnetic	20,000	1.02
Ti-6Al-4V	Paramagnetic	1.81×10^{-4}	1.00005
Al-bronze(C95400)	Paramagnetic	9.63×10^{-6}~2.11×10^{-5}	1.07

VII. RESULTS

The force-displacement curves of titanium alloy, aluminum bronze, and 301 stainless steel spring plates are compared in Figure 6. These curves highlight the "trip force," which is the maximum force in the return path and a key parameter for spring plate performance. The curves show different displacements (travel heights) in the actuation model, with each material generating unique dome curvatures (d-ring) during the punching process due to their distinct material properties. Spring plates made from different materials vary geometrically in terms of travel height, thickness, and other dimensions. Ductility, which controls material deformation, was found to influence these variations. Ductility allows metals to plastically deform without becoming brittle, and materials with higher ductility can undergo more stretching.

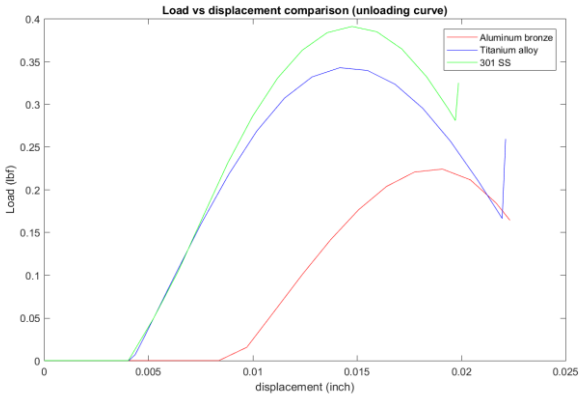

Fig. 6 Load vs displacement comparison

To investigate ductility's impact, a comparison of thickness and curvature for the same geometric values is presented in Table 3. The results show that 301 stainless steel's thickness aligns closely with the design value, whereas titanium's is farther from the target. Ductility values in Table 1 show that 301 stainless steel has the highest ductility, while titanium has the lowest. These variations suggest that ductility significantly affects the punching process of nonlinear spring plates, potentially influencing their fatigue life cycle.

TABLE 3 COMPARISON OF DUCTILITY EFFECT

Material	Travel height(in)	Thickness (in)	Travel height(in)	Thickness(in)
Design value	1.91E-01	3.00E-02	2.01E-01	3.00E-02
Ti-6Al-4V	2.30E-01	2.30E-03	2.25E-01	2.20E-03
Al-bronze	2.20E-01	2.60E-03	2.11E-01	2.40E-03
301 Stainless steel	1.90E-01	2.70E-03	2.00E-01	2.77E-03

Fatigue life was analyzed using the universal slope equation, with results shown in Table 4.

TABLE 4 FATIGUE LIFE EQUATION

Material	Fatigue equation
301 stainless steel	$N_f = 3.041\times10^{-15}\times\Delta\varepsilon^{-9.009}$
Ti-6Al-4V	$N_f = 3.6402\times10^{-16}\times\Delta\varepsilon^{-10.284}$
Al-bronze(C95400)	$N_f = 2.680349\times10^{-16}\times\Delta\varepsilon^{-9.2421}$

Cracks were observed to initiate at the crotch region of the spring plates. Fatigue analysis (Table 5) revealed that titanium alloy spring plates fail first,

exhibiting the shortest fatigue life, while aluminium bronze plates show a longer fatigue life.

TABLE 5 FATIGUE LIFE COMPARISON

Material	Average Minimum Life	Minimum Life
301 stainless steel	110441	24675
Ti-6Al-4V	29922	13280
Al-bronze(C95400)	154323	25165

This finding aligns with the manufacturer's testing. Further investigation into titanium alloy's fatigue life revealed that it generates higher strains, as shown in Figure 7, which correlates with its lower fatigue life.

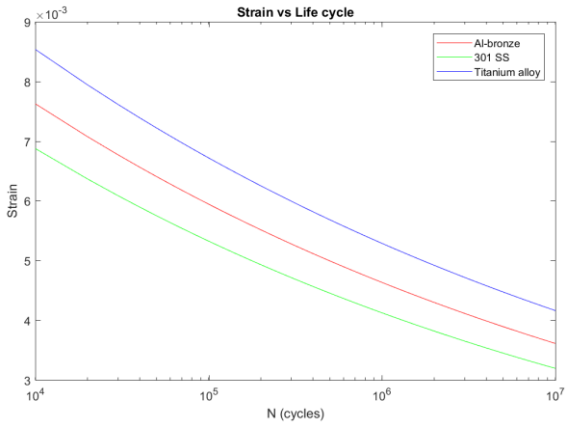

Fig. 7 Fatigue life comparison

This suggests that titanium can be classified as a plastically deformed material. As noted by Manson, Coffin, and Basquin, ductility plays a crucial role in fatigue under plastic deformation. Therefore, more studies are needed to further explore the influence of ductility and strain on the failure of titanium alloy spring plates. The strong geometric nonlinearity of the spring plates causes snap-through buckling under load, leading to a

temporary loss of equilibrium and kinetic energy generation. The energy balance in the actuation model, defined by Equation (7), was investigated. For both static and dynamic implicit analysis, total energy was found to be identical, though an initial kinetic energy was required to compress the spring plate, resulting in a higher initial total energy in both analyses. Contact dissipation energies were larger in the static model compared to the dynamic model. Figure 9 shows that static analysis generates more viscous dissipation (ALLVD) than kinetic analysis. Furthermore, Figure 10 highlights that kinetic energy generated in the dynamic analysis due to snap-through buckling is minimal, while the static solver produced no kinetic energy throughout the analysis. The plastic dissipation energies in both analyses were identical (Figure 11), indicating that the effect of snap-through buckling on kinetic energy in the static analysis is negligible.

VIII. CONCLUSION

This study has identified key factors in selecting a nonmagnetic material for spring plates, highlighting the performance differences observed through finite element analysis and material property evaluations. The study found that the titanium alloy nonlinear spring plate exhibited the lowest trip force compared to other materials. Fatigue life analysis revealed that while aluminum alloy spring plates had the highest average minimum life before crack initiation, the fatigue life cycle performance of titanium alloy was comparatively lower. The fatigue life calculations indicated that the plastic part of the universal slope model was governed by ductility, which also influenced the geometric shapes of the spring plates in the forming model. Additionally, the fatigue life cycle of titanium alloy spring plates was primarily controlled by strain and ductility.

REFERENCES

[1] Bacha A, Daniel D, Klocker H, "Crack deviation during trimming of aluminum automotive sheets," Journal of Material Processing Technology 2010;210:1885-97

[2] A.L. Gurson, "Continuum Theory of Ductile Rupture by Void Nucleation and Growth: Part 1 - Yield Criteria and Flow Rules for Porous Ductile Media," J Eng Math Tech, Trans ASME 1977; 9:2-15.

[3] V. Tvergaard, A. Needleman, "Analysis of the cup-cone fracture in a round tensile bar," Acta Metal Mater 1984;32:157-69

[4] K. Nahshon, J. Hutchinson, "Modification of the Gurson model for shear failure," Eur J Mech A/Solids 2008;27:1-17

[5] K. Nielson, V. Tvergaard, "Ductile shear failure or plug failure of spot welds modelled by modified Gurson model," Eng Fract Mech 2010,77:1031-47

[6] M. Achouri, G. Germain, P.D. Santo, D. Saidane, “Experimental and numerical analysis of micromechanical damage in the punching process for high-strength low-alloy steels,” Materials and Design 56 (2014) 657-670

[7] D.J, Smith, G.H. Farrahi, W.X. Zhu, C.A. McMahon, “ Experimental measurement and finite element simulation of interaction between residual stresses and mechanical loading,” International Journal on Fatigue 23 (2001) 293-302

[8] K. M. Galib, Shah Rahman, “Finite element analysis of hybrid and non-hbyrid laminate composite ” International Journal of Scientific Research and Engineering Development, 2023 **10.5281/zenodo.14047045**

[9] S.S. Manson, M.H. Hirschberg, “The role of Ductility, Tensile Strength and Fracture Toughness in Fatigue,”

[10] S. Roy, “Fatigue Simulation Technologies of Cold Expansion Processed Aerospace Aluminum and Rail Steel Holes Using the Extended Finite Element Method”, Washington State Univ, (2021). https://hdl.handle.net/2376/119050

[11] S. Roy and D. Kim, “Effect of Material Property and Hole Cold Expansion Rate on Fatigue Crack Initiation and Propagation on 2024-T351 Aluminum Alloy Holes” IMECE2020 – Vir. Conf (2021). doi: 10.13140/RG.2.2.25665.36968 https://imece.secure-platform.com/a/solicitations/121/sessiongallery/6004/application/56948

[12] U. Muralidharan, S.S. Manson, “A Modified Universal Slopes Equation for Estimation of Fatigue Characteristics of Metals”

[13] J.J. Lucas, P.P. Konieczny, ”Relation between alpha grain size and Crack initiation on Fatigue Strength in Ti-6Al-4v,” Metal Trans., 1971, 2 (March)

[14] Shabnam Hosseini, H. Arabi, M. Tamizifar and A. Zeyaei, “Effect of tensile strength on behavior and notch sensitivity of Ti-6Al-4v”, Iranian journal of materials science and engineering, Vol.3, Winter &Spring 2006, PP.12-16

[15] M. E. McHENRY and D. E. Laughlin, “NANO-SCALE MATERIALS DEVELOPMENT FOR FUTURE MAGNETIC APPLICATIONS p”.

[16] W. Robertson, B. Cazzolato, and A. Zander, “Theoretical analysis of a non-contact spring with inclined permanent magnets for load-independent resonance frequency,” *J. Sound Vib.*, vol. 331, no. 6, pp. 1331–1341, Mar. 2012, doi: 10.1016/j.jsv.2011.11.011.

[17] E. Bonisoli and A. Vigliani, “Passive elasto-magnetic suspensions: nonlinear models and experimental outcomes,” *Mech. Res. Commun.*, vol. 34, no. 4, pp. 385–394, Jun. 2007, doi: 10.1016/j.mechrescom.2007.02.005.

[18] E. F. Kneller and R. Hawig, “The exchange-spring magnet: a new material principle for permanent magnets,” *IEEE Trans. Magn.*, vol. 27, no. 4, pp. 3588–3560, Jul. 1991, doi: 10.1109/20.102931.

[19] C. S. Lee, K. A. Lee, D. M. Li, S. J. Yoo, and W. J. Nam, “Microstructural influence on fatigue properties of a high-strength spring steel,” *Mater. Sci. Eng. A*, vol. 241, no. 1–2, pp. 30–37, Jan. 1998, doi: 10.1016/S0921-5093(97)10469-5.

[20] W. J. Nam, C. S. Lee, and D. Y. Ban, “Effects of alloy additions and tempering temperature on the sag resistance of Si–Cr spring steels,” *Mater. Sci. Eng. A*, vol. 289, no. 1–2, pp. 8–17, Sep. 2000, doi: 10.1016/S0921-5093(00)00928-X.

[21] M. S. Htun, S. T. Kyaw, and K. T. Lwin, “Effect of Heat Treatment on Microstructures and Mechanical Properties of Spring Steel”.

[22] I. Khader *et al.*, “Characterization of a silicon nitride ceramic material for ceramic springs,” *J. Eur. Ceram. Soc.*, vol. 40, no. 10, pp. 3541–3554, Aug. 2020, doi: 10.1016/j.jeurceramsoc.2020.03.046.

[23] A. M. A. Hossain, N. Masud, S. Roy, and M. Ali, "Investigation of voltage storage capacity for the variation of electrode materials in microbial fuel cells with experimentation and mathematical modelling," Int. Jour. of Water Res. and Env. Eng., 14(4), pp. 97-109 (2022). https://doi.org/10.5897/IJWREE2022.1037

[24] S. Roy, A. M. A. Hossain, S. Roy, M. Mamun, “Parametric Analysis of Wind Load on the Cross-Sections of Different Types of Building Geometry.”

[25] J. L. Favero, A. R. Secchi, N. S. M. Cardozo, and H. Jasak, “Viscoelastic flow analysis using the software OpenFOAM and differential constitutive equations,” *J. Non-Newton. Fluid Mech.*, vol. 165, no. 23–24, pp. 1625–1636, Dec. 2010, doi: 10.1016/j.jnnfm.2010.08.010.

[26] A. Hillerborg,” The theoretical basic of a method to determine the fracture energy G_F of concrete,” Material and Structures, July 1985, Volume 18, Issue 4, pp 291-296

[27] http://abaqus.software.polimi.it/v6.13/books/usb/default.htm?startat=pt05ch24s02abm42.html

[28] https://classes.engineering.wustl.edu/2009/spring/mase5513/abaqus/docs/v6.6/books/gsx/default.htm?startat=ch03s07.html

[29] D.A. Leaonhardt, “A method for fatigue life prediction of complex formed geometries.”